JSAT IVCST 2021
Journal of Science and Agricultural Technology
Research Article
https://doi.org/10.14456/jsat.2022.1
e-ISSN 2730-1532, ISSN 2730-1524

Land surface temperature estimation for Buriram town municipality, Thailand

Pantip Piyatadsananon[1*] and Ekkaluk Salakkham[1]

[1]School of Geoinformatics, Institute of Science, Suranaree University of Technology, University Avenue Muang District, Nakhon Ratchasima, 30000, Thailand

***Corresponding author**: pantip.p@sut.ac.th*
Received: October 13, 2021. Accepted: February 14, 2022.

ABSTRACT

Land Surface Temperature (LST) has long been monitored and studied; however, the most reliable method of estimating the LST has yet to be examined regarding the mixed land-use types over a small city. This research explores an optimum method for Land Surface Temperature (LST) estimation in a city using the data from LANDSAT-8. Four favored LST retrieval approaches, the Radiative Transfer Equation-based method (RTE), the Improved Mono-Window method (IMW), the Generalized Single-Channel method (GSC), and the Split-Window algorithm (SW), were used to estimate the LST over Buriram Town Municipality, Thailand. The calculated LST from these four methods was compared with ground-based temperature data of 100 measured sites over the study area on the same date and time as the employed Landsat-8 data. The lowest Normalized Root Means Square Error (NRMSE) was considered to identify the optimum method of the LST estimation. The SW algorithm provides the lowest NRMSE value (0.114), followed by the RTE (0.171), the IMW algorithm (0.181), and the GSC (0.219). As a result, the SW algorithm is the optimum method in LST estimation for Buriram Town Municipality. The SW algorithm mainly eliminates atmospheric effects based on differential absorption in two thermal bands, which have shown the smallest error in the retrieval of LST. The explored optimal method will benefit GIS specialists working for Buriram local government to conduct the best practice to monitor the LST over the city. The other local governments could consider the SW algorithm to monitor the LST over their small cities with similar contents.

Keywords: split-window, Landsat-8, land surface temperature, thermal bands, Buriram

INTRODUCTION

Land Surface Temperature (LST) is an essential variable for estimating radiation and energy budgets associated with mainland surface processes (Holmes et al., 2013; Orhan et al., 2014; Wu et al., 2013). Knowledge of LST distribution can provide useful information about the surface's physical properties and climate, which have a role in a variety of fields, including land-atmosphere energy budget (Weng and Fu, 2014; Wu et al., 2015), climate change (Avdan and Jovanovska, 2016; Weng et al., 2014; Wu et al., 2015), hydrological cycle (Avdan and Jovanovska, 2016; Bendib et al., 2016; Wu et al., 2015), evapotranspiration (Bendib et al., 2016; Weng et al., 2014), and urban climate (Bendib et al., 2016; Mechri et al., 2014; Weng and Fu, 2014). LST data from satellite remote sensing provides denser spatial sampling intervals than those taken at ground sites (Zhou et al., 2015). Data from the LANDSAT series is widely used for retrieving the LST, according to the downloadable free data from the USGS website, regular revisit times, and long-term recorded data captured by two onboard instruments: the Operational Land Imager (OLI) and the Thermal Infrared Sensor (TIRS) (Salakkham and Piyatadsananon, 2020). Based on the TIR bands of Landsat-8, the available data is appropriate to apply the split-window algorithms (SW) (Jimenez-Munoz et al., 2014) and three LST estimation methods of single-channel methods, Radiative Transfer Equation-based method (RTE), the Improved Mono-Window method (IMW), and the Generalized Single-Channel method (GSC) (Li et al., 2013). Weng et al. (2004) indicated that the emissivity estimation for ground objects from passive sensor data could be measured using different technics. Liu et al. (2006) and Coll et al. (2010) noted that LST estimation was performed over the large, fully vegetated surface, bare surfaces, and deserts, with relatively homogeneous test sites avoiding uncertainty due to spatial heterogeneity. Therefore, an optimal method to estimate the actual temperature from mixed land-use types in a pixel of Landsat-8 data has to be examined and criticized. This study aimed to explore the optimum method in LST estimation over four favoured algorithms, RTE, IMW, GSC, and SW, regarding their wide use in these recent years. As a result, the four LST retrieval algorithms were criticized and explored the limits of the applied parameters. This study benefits the GIS specialists

working for local government to follow the best practice for the LST estimation over a city. Later, provincial officers can use the explored results from the optimal method to monitor the LST over a small and diverse city, such as Buriram Town Municipality.

MATERIALS AND METHODS

1. Land Surface Temperature (LST) estimation

Four LST (Land Surface Temperature) estimation algorithms have been typically employed in recent decades in response to remote sensing data. The RTE and IMW were developed by Wang et al. (2015). The GSC and SW were developed by Jimenez-Munoz et al. (2014). The first one the Radiative transfer equation-based method (RTE), was developed by Wang et al. (2015) with the concern of radiative transfer equation based on Plank's law inversion (Skokovic et al., 2014). The atmospheric profile was extracted from the NCEP (National Centers for Environmental Prediction) dataset and used to simulate atmospheric transmittance, up-welling, and down-welling radiance from the Moderate-resolution atmospheric Transmisi (MODTRAN) model (Salakkham and Piyatadsananon, 2020). The expresbrackets the RTE is,

$$LST = \frac{C_2}{\lambda \ln\left\{\frac{C_1}{\lambda^5[\ ]} + 1\right\}} \quad (1)$$

Where L_{sensor} is thermal radiance at the sensor level, ε is land-surface emissivity, τ is atmospheric transmissivity, L_u and L_d are up-welling and down-welling atmospheric radiance, respectively, and C_1 and C_2 are the constant-coefficients.

Later, Qin et al. (2001) developed the mono-window algorithm. It was used for estimating the LST from LANDSAT-5 to avoid dependence on radio-sounding in the RTE method (Sobrino et al. 2004). Consequently, Wang et al. (2015) developed the mono-window into the Improved Mono-Window (IMW) method for obtaining LST from LANDSAT-8 in 2015 (Salakkham and Piyatadsananon, 2020), as shown in the following expression.

$$LST = \frac{1}{C}\left[a(1 - C - D) + \left(b(1 - C - D) + C + D\right)T_B - DT_a\right] \quad (2)$$

With $C = \varepsilon\tau$

$D = (1 - \tau)[1 + (1 - \varepsilon)\tau]$

Where a and b are constant coefficients, ε is the land surface emissivity, τ is the total atmospheric transmissivity, T_B is the at-sensor brightness temperature, and T_a is the mean atmospheric temperature.

In 2003, Jimenez-Munoz and Sobrino (2003) initially developed the Generalized Single-Channel (GSC) algorithm to estimate the LST from LANDSAT-5. It was further developed in 2014 to obtain LST from LANDSAT-8, shown in the following expression Salakkham and Piyatadsnanon, 2020).

$$LST = \gamma\left[\varepsilon^{-1}\left(\psi\ L_{sensor}\ \psi_2\right) + \psi_3\right] + \delta \quad (3)$$

$$\text{With } \gamma = \frac{T_B^2}{b_\gamma L_{sensor}} \quad (4)$$

$$\delta = T_B - \frac{T_B^2}{b_\gamma} \quad (5)$$

Where L_{sensor} is thermal radiance at the sensor level, b_γ equals 1,324 K, and 1,199 K for TIRS -1 (Band 10) and TIRS -2 (Band 11), respectively, T_B is at-sensor brightness temperature, ε is the land surface emissivity, and ψ_1, ψ_2, ψ_3 an be obtaned as a function of the total atmospheric water vapor content (w).

Eventually, the split-window algorithm, developed by Jimenez-Munoz et al. (2014), is shown in the following expression.

$$T_s = T_i + C_1(T_i - T_j) + C_2(T_i - T_j)^2 + C_0 + (C_3 + C_4 w)(1-\varepsilon) + (C_5 + C_6 w)\Delta\varepsilon \quad (6)$$

Where C_0 to C_6 are the split window coefficients, T_i and T_j are at-sensor brightness temperatures of Band i and j, respectively, ε is the land surface emissivity obtained from $\varepsilon = 0.5\ (\varepsilon_i + \varepsilon j)$ and $\Delta\varepsilon = (\varepsilon_i - \varepsilon_j)$.

It is noted that the near-surface air temperature (T_0) and relative humidity were received from Huai Rat Station near Buriram Town Municipality (approximately twelve kilometers). As mentioned in a report by Salakkham and Piyatadsananon (2020) that near-surface air temperature (T_0) and relative humidity can be found on the Hydro and Agro Informatics Institute (HAII) website (Salakkham and Piyatadsananon, 2020). The parameters were used in the water vapor content calculation and estimation developed by Liu and Zhang (2011) as equation (7). The water vapor content has been used in the transmittance calculation for the IMW algorithm, the atmospheric function,

the GSC algorithm, and the SW algorithm (Salakkham and Piyatadsananon, 2020). This parameter has also been used in the atmospheric temperature (T_a) calculation, an essential parameter of the IMW algorithm.

$$w_i = \left\{0.59 \times RH \times exp\left[\frac{17.27 \times (T_0 - 273.15)}{237.3 + (T_0 - 273.15)}\right]\right\} + 0.1697 \quad (7)$$

Where w_i is the water vapor content (g cm^{-2}), T_0 is the near-surface air temperature (K), and RH is the relative humidity (Decimal). The water vapor content, near-surface air temperature, and relative humidity are the average values.

The transmittance, up-welling, and down-welling atmospheric radiance were obtained from the NASA atmospheric correction parameter calculator (Salakkham and Piyatadsananon, 2020). It is clearly shown that the calculator uses the National Center for Environmental Prediction (NCEP) to model global atmospheric profiles, which are interpolated to a particular date, time, and location as input for the MODTRAN radiative transfer code, and as a suite of the integrative algorithm to infer the up-welling, down-welling radiances and site-specific transmission (Salakkham and Piyatadsananon, 2020). The profiles resulting from time interpolation provide the closest latitudinal and longitudinal positions or specific locations (Vlassova et al., 2014).

2.Methods

2.1 Study Area

Buriram province is in the Northeastern region of Thailand. It has flourished over the last decade as a sports city in the country. A mega-sports complex, which contains a massive stadium for football, a motor racing track, and several ongoing construction projects, attracts many tourists and drives up the demand for further construction across Buriram Town Municipality (Buriram World, 2016; Tourism Authority of Thailand, 2017). The local government has planned to improve the Town Municipality to City Municipality to support urbanization (Buriram World, 2016). With six square kilometers for over 30,000 families living in the municipality, Buriram municipality is the most crowded city (around five-thousand population in a square kilometer) in the Northeastern region (The Bureau of Registration Administration, 2018). The maximum temperature in the summer has increased to more than 40 ºC (in 2013 – 2018) (Buriram Statistic Office, 2018).

2.2 Data collection

The data used in the LST estimation of this study are listed in table 1 with their sources.

Table 1. Data used in the study.

Data	Date	Sources
LANDSAT-8 data Path /Row: 128 /50	Jan 21st, Feb 6th, Mar 26th, Apr 11th, 2018	U.S. Geological Survey (USGS)
UAV image (GSD = 5cm.)	Mar-Apr, 2018	Surveying between 10-11 am.
Ground-based temperature data	Jan 21st, Feb 6th, Mar 26th, Apr 11th, 2018	Surveying between 10-11 am.
Atmospheric parameters • Air temperature • Relative humidity	Jan 21st, Feb 6th, Mar 26th, Apr 11th, 2018 Between 10-11 am.	Hydro and Agro Informatics Institute (HAII) website
Atmospheric parameters • Transmittance • Up-welling and down-welling atmospheric radiance	Jan 21st, Feb 6th, Mar 26th, Apr 11th, 2018	NASA atmospheric correction parameter calculator website

The atmospheric parameters used in the LST estimation of four methods are listed in table 2.

Table 2. Atmospheric parameters used in LST estimations.

		Jan 21st	Feb 6th	Mar 26th	Apr 11th
Temperature (T_0) (K)		303.9	293.1	302.9	309.3
Air Temperature (T_0) (ºC)		30.75	19.95	29.75	36.15
Relative Humidity		0.63	0.60	0.65	0.44
Water Vapor Content		2.86	1.52	2.79	2.72
Methods	**Atmospheric Parameters**	**Jan 21st**	**Feb 6th**	**Mar 26th**	**Apr 11th**
RTE	Transmittance (τ) [a]	0.53	0.80	0.54	0.60
	Up-welling	3.92	1.63	3.78	3.56
	Down-welling	6.00	2.67	5.86	5.65
IMW	Atmospheric Temperature (T_a)(K)	296.69	286.79	295.78	301.65
	Transmittance (τ) [b]	0.65	0.80	0.65	0.65
GSC	Atmospheric Function (ψ_1)	1.42	1.15	1.41	1.39
	Atmospheric Function (ψ_2)	-7.25	-2.97	-6.99	-6.70
	Atmospheric Function (ψ_3)	3.69	1.81	3.60	3.49
SW	Water Vapor Content	2.86	1.52	2.79	2.72

Note: [a] Transmittance, up-welling, and down-welling used in the RTE method were obtained from NCEP
[b] The transmittance used in IMW was calculated based on the mono-window method.

2.3 Procedures

The conceptual procedure of this study is illustrated in figure 2. It consists of three major parts, (1) ground-based temperature measurement, (2) LST estimation, and (3) the comparison between ground-based temperature data and the calculated LST data from the Landsat 8 data. Eventually, the optimum method of LST estimation was then identified by considering the lowest calculated NRMSE values.

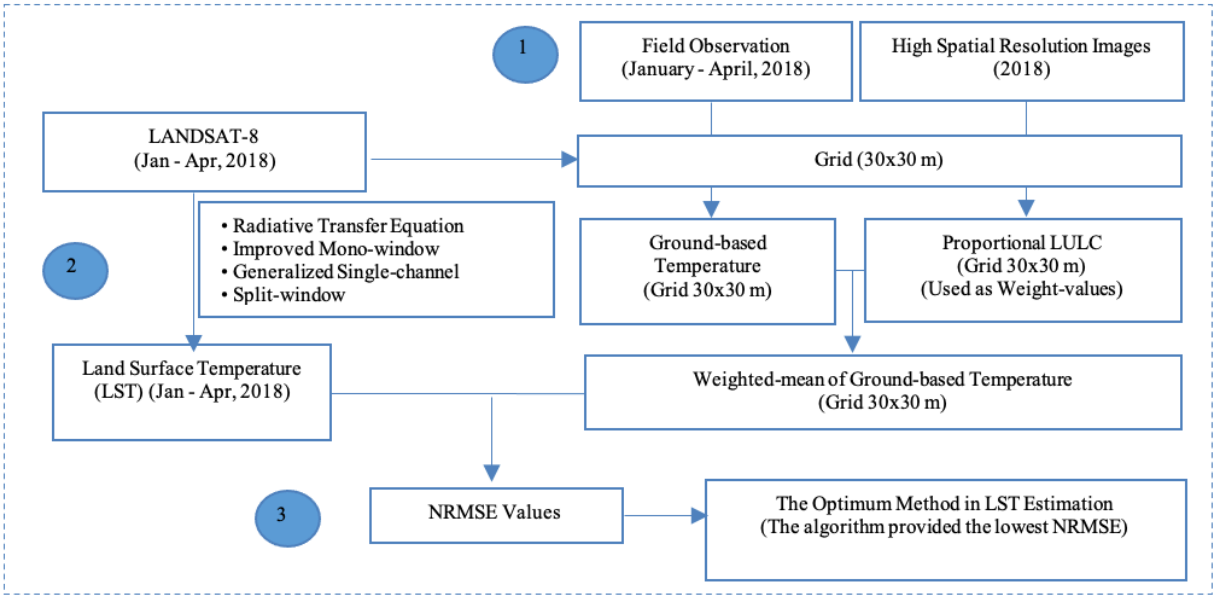

Figure 1. The conceptual procedure of the study.

2.4 Ground-based temperature measurement

Basically, the LANDSAT-8 image contains 30x30 meter-grids, whereas the thermal band image consists of 100x100 meter-grids. Therefore, an aggregated pixel of 3x3 pixels (90x90 m.) of OLI was assembled to be a pixel size of the Thermal image (100x100 m.). The Land-Use and Land-Cover (LULC) types within a thermal pixel (100x100 m.) were classified by visual interpretation technic on the high-resolution image from the UAV. The LULC within a thermal grid cell was assessed as the weighted value regarding the proportion of the mixed LULC. The high-resolution image from the UAV was also used as the based map for planning the ground-based temperature measurement. A hand-held digital thermometer was calibrated every time before measuring the LST in the sample sites. One hundred sample sites were measured and recorded the land surface temperature in the center of the 3x3 pixels of OLI, or 90x90 m. of thermal bands during 10-11 am. on Jan 21st, Feb 6th, Mar 26th, and Apr 11th, 2018.

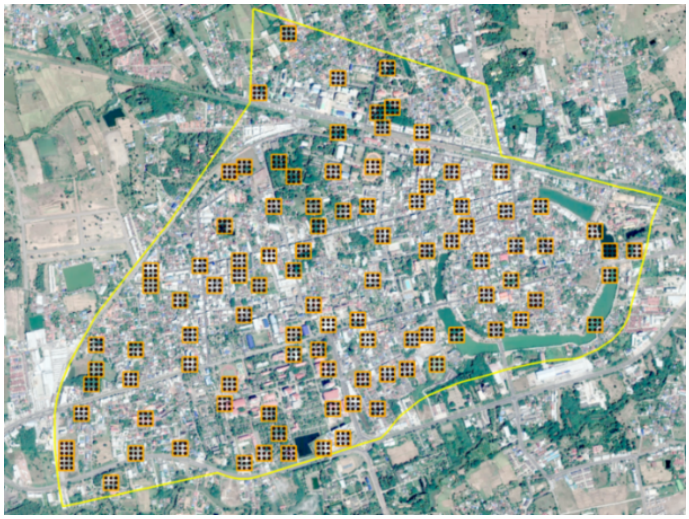

Figure 2. The 100 sample sites (small orange grids) over Buriram Municipality (yellow boundaries).

2.5 Accuracy assessment

The optimum method in the LST extraction, RTE, IMW, GSC, and SW algorithm, as equation (1) – (7), were used in the calculations. Eventually, the method that provides the lowest NRMSE values is considered an optimum method for the LST estimation of Buriram Town Municipality.

$$NRMSE = \frac{RMSE}{maximum\ observation - minimm\ observation} \quad (8)$$

Where maximum and minimum observations are the maximum and minimum temperature of in-situ data.

RESULTS AND DISCUSSION

The result from the split-window technique shows a more complex surface than others (Figure 3). As a reason, two thermal infrared channels have narrower bandwidths, which can capture finer land surface information response to studies by Li, et al. (2013) (Wenbin et al., 2013; Du et al., 2015). The accuracy assessment was examined to explore the optimum method in the LST estimation by considering the lowest NRMSE value of each method. The RMSE and NRMSE values as shown in table 3 and figure 4. The SW method eliminates atmospheric effects based on differential absorption in two thermal bands with narrow bandwidths in the thermal infrared (Salakkham and Piyatadsananon, 2020). As supported by the studies of Caselles et al. (1998) and Rozenstein et al. (2014), whether two separating narrow thermal infrared presents the smallest error in the LST retrieval. However, the SW algorithm is sensitive to water vapor content and coefficients. Typically, the coefficients used in the SW algorithm are based on the series of studies (Jimenez-Munoz and Sobrino, 2008; Jimenez-Munoz et al. 2014; Jin et al., 2015). In addition, the coefficients depend on the atmospheric state, while the fixed values were sometimes utilized, causing significant errors to the results, as highlighted in a study by Vazquez et al. (1997).

On the other hand, the single-channel methods, RTE, IMW, and GSC algorithms, rely on the accuracy of the radiative transfer model and the atmospheric profiles representing the actual state of the atmosphere over the studies area at the orbital time (Salakkham and Piyatadsananon, 2020). The error of the RTE algorithm comes from the atmospheric model used in the calculation of the atmospheric parameters. Since the study area is located in the tropical zone, the available model is the NCEP model presenting the mid-latitude summer and mid-latitude winter models, as same as the discussion in a study by Jimenez-Munoz et al. (2009). The error from the IMW algorithm comes from the essential atmospheric parameters used in this algorithm. There is no reference source in near-ground air temperature (T_0) acquisition, used in the sufficient atmospheric temperature (T_a). The sufficient atmospheric temperature (T_a) is an essential practical issue used to retrieve LST over a large area, as emphasized by Cristobal et al. (Cristobal et al. 2009). Lastly, the GSC algorithm provides a higher error than other methods. The basis of this algorithm relies on the estimation of the so-called atmospheric function, which is assumed to be dependent only on water vapor content values (Salakkham and Piyatadsananon, 2020). Chen et al. (2011) and Cristobal et al. (2009) explained that the atmospheric functions might be obtained more precisely from water vapor content and air temperature.

Table 3. NRMSE Values of the LST estimation methods

Date	NRMSE			
	RTE	IMW	GSC	SW
Jan 21st, 2018	0.454	0.613	0.650	0.227
Feb 6th, 2018	0.702	0.317	0.671	0.473
Mar 26th, 2018	0.246	0.416	0.509	0.218
Apr 11th, 2018	0.165	0.226	0.202	0.132
Overall NRMSE	0.171	0.181	0.219	0.114

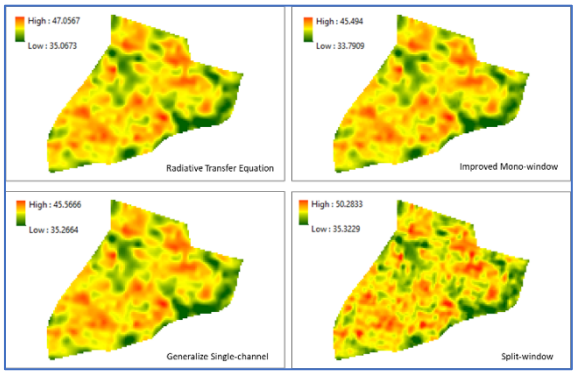

Figure 3. LST calculated by four methods.

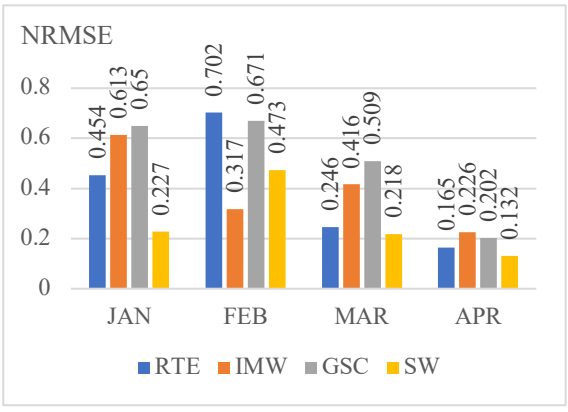

Figure 4. NRMSE values, monthly results.

CONCLUSIONS

It can be concluded that the SW algorithm provided the lowest NRMSE value (0.114); nevertheless, the IMW algorithm provided a better result than the SW algorithm on Feb 6th, 2018. It is noticeable that the average temperature on Feb 6th, 2018 was, dramatically dropped to 19.95 °C, shown in table 2, so it caused the lowest water vapor content

(1.52 g cm^{-2}) in Feb 2018. For this reason, the critical point is that the amount of atmospheric water vapor content data plays an essential role in calculating accuracy. This parameter is typically estimated by considering the near-surface air temperature and relative humidity values (Salakkham and Piyatadsananon, 2020). To enhance the accuracy of all practiced algorithms, it is recommended to obtain the near-surface air temperature and relative humidity in-situ of the study area. Apart from the atmospheric correction parameters, the surface emissivity must also be considered to enhance the accuracy of the LST retrieval. The study area, Buriram Town Municipality, appears as heterogeneous LULC within a thermal-image pixel, causing different spectrum reflectance. Regarding coarse spatial resolution, it is strongly affected by mixed pixels, whereby each pixel comprises a mixture of two or more land cover types (Feng et al., 2015). Therefore, the SW algorithm is recommended for the LST estimation in a small city like Buriram municipality. It can be done regularly using the Landsat-8 data with the sub-pixel technique, which can monitor the LST in small cities. Considering the limitation of the parameters used in the SW method, it is suggested that a local weather station in the city should be identified to provide the near-surface air temperature and relative humidity values. The explored optimum method for the LST estimation from this study will be useful to GIS specialists who are working for the local government to conduct this technic to prevent the urban heat island (UHI) in small cities with similar contents.

REFERENCES

Avdan, U., and Jovanovska, G. 2016. Algorithm for automated mapping of the land surface temperature using Landsat-8 satellite data. Journal of Sensors. 2016: 1-8.

Bendib, A., Dridi, H., and Kalla, M. I. 2016. Contribution of Landsat-8 data for the estimation of land surface temperature in Batna City, Eastern Algeria. Geocarto International. https://doi.org/10.1080/10106049.2016.1156167

Buriram Statistic Office. 2018. Monthly temperature and atmospheric pressure data 2013-2018. Retrieved from http://buriram.old.nso.go.th/nso/project/search_option/search_result.jsp

Buriram World. 2016. Retrieved from https://www.buriramworld.com/

Caselles, V., Rubio, E., Coll, C., and Valor, E. 1998. Thermal band selection for the PRISM instrument 3: Optimal band configurations. Journal of Geophysical Research. 103: 17057-17067.

Chen, F., Zhao, X., Ye, H., and Hu, H. 2011. Retrieving land surface temperature from Landsat TM using different atmospheric products as ancillary data. Paper presented at the Spatial Data Mining and Geographic Knowledge Services (ICSDM), Fuzhou, China.

Coll, C., Galve, J. M., Sanchez, J. M., and Caselles, V. 2010. Validation of Landsat-7/ETM+ thermal-band calibration and atmospheric correction with ground-based measurements. IEEE Transactions on Geoscience and Remote Sensing. 48(1): 547-555.

Cristobal, J., Jimenez-Munoz, J. C., Sobrino, J. A., Ninyerola, M., and Pons, X. 2009. Improvements in land surface temperature retrieval from the Landsat series thermal band using water vapor and air temperature. Journal of Geophysical Research. 114. https://doi.org/10.1029/2008JD010616

Du, C., Ren, H., Qin, Q., Meng, J., and Zhao, S. 2015. A practical split-window algorithm for estimating land surface temperature from Landsat-8 data. Remote Sensing. 7: 647-665.

Feng, X., Foody, G., Aplin, P., and Gosling, S. N. 2015. Enhancing the spatial resolution of satellite-derived land surface temperature mapping for urban areas. Sustainable Cities and Society. 19: 341-348.

Holmes, T. R. H., Crow, W. T., Yilmaz, M. T., Jackson, T. J., and Basara, J. B. 2013. Enhancing model-based land surface temperature estimates using multiplatform microwave observations. Journal of Geophysical Research: Atmospheres, 118: 577-591.

Jimenez-Munoz, J. C., Cristobal, J., Sobrino, J. A., Soria, G., Ninyerola, M., and Pons, X. 2009. Revision of the single-channel algorithm for land surface temperature retrieval from Landsat thermal-infrared data. IEEE Transactions on Geoscience and Remote Sensing. 47(1): 339-349.

Jimenez-Munoz, J. C., and Sobrino, J. A. 2003. A Generalized single-channel method for retrieving land surface temperature from remote sensing data. Journal of Geophysical Research. 108: 1-9.

Jimenez-Munoz, J. C., and Sobrino, J. A. 2008. Split-window coefficients for land surface temperature retrieval from low-resolution thermal infrared sensors. IEEE Geoscience and Remote Sensing Letters. 5(4): 806-809.

Jimenez-Munoz, J. C., Sobrino, J. A., Skokovic, D., Matter, C., and Cristobal, J. 2014. Land surface temperatures retrieval methods from Landsat-8 thermal infrared sensor data. IEEE Geoscience and Remote Sensing Letters. 11(10): 1840-1843.

Jin, M., Li, J., Wang, C., and Shang, R. 2015. A practical split-window algorithm for retrieving land surface temperature from Landsat-8 data and a case study of an urban area in China. Remote Sensing. 7: 4371-4390.

Li, Z. L., Tang, B. H., Wu, H., Ren, H., Yan, G., Wan, Z., and Sobrino, J. A. 2013. Satellite-derived land surface temperature: Current status and perspective. Remote Sensing of Environment. 131: 14-37.

Liu, L., and Zhang, Y. 2011. Urban heat island analysis using the Landsat TM data and ASTER data: A case study in Hong Kong. Remote Sensing. 3: 1535-1552.

Liu, Y., Hiyama, T., and Yamaguchi, Y. 2006. Scaling of land surface temperature using satellite data: A case examination on ASTER and MODIS products over a heterogeneous Terrain Area. Remote Sensing of Environment. 105: 115-128.

Mechri, R., Ottle, C., Pannekoucke, O., and Kallel, A. 2014. Genetic particle filter application to land surface temperature downscaling. Journal of Geophysical Research: Atmospheres. 119: 2131-2146.

Orhan, O., Ekercin, S., and Dadaser-Celik, F. 2014. Use of Landstat land surface temperature and vegetation indices for monitoring drought in the Salt Lake Basin Area, Turkey. The Scientific World Journal. 2014: 1-11.

Qin, Z., Karnieli, A., and Berliner, P. 2001. A mono-window algorithm for retrieving land surface temperature from Landsat TM data and its application to the Israel-Egypt border region. International Journal of Remote Sensing. 22(18): 3719-3746.

Rozenstein, O., Qin, Z., Derimian, Y., and Karnieli, A. 2014. Derivation of land surface temperature for Landsat-8 TIRS using a split-window algorithm. Sensors. 14: 5768-5780.

Salakkham, E., and Piyatadsananon, P. 2020. The optimum method for urban land surface temperature estimation. preprints 2020. Seminar Report. Suranaree University of Technology.

Skokovic, D., Sobrino, J. A., Jimenez-Munoz, J. C., Soria, G., Julien, Y., Matter, C., and Cristobal, J. 2014. Calibration and validation of land surface temperature for Landsat-8 TIRS sensor. Retrieved from https://earth.esa.int/documents/700255/2126408/ESA_Lpve_Sobrino_2014a.pdf

Sobrino, J. A., Jimenez-Munoz, J. C., and Paolini, L. 2004. Land surface temperature retrieval from Landsat TM 5. Remote Sensing of Environment. 90: 434-440.

Tourism Authority of Thailand. 2017. Buriram. Retrieved from https://www.tourismthailand.org/About-Thailand/Destination/Buri-Ram

Vazquez, D. P., Reyes, F. J. O., and Arboledas, L. A. 1997. A comparative study of algorithms for estimating land surface temperature from AVHRR data. Remote Sensing of Environment. 62: 215-222.

Vlassova, L., Perez-Cabello, F., Nieto, H., Martin, P., Riano, D., and Riva, J. d. l. 2014. Assessment of methods for land surface temperature retrieval from Landsat-5 TM images applicable to multiscale tree-grass ecosystem modeling. Remote Sensing. 6: 4345-4368.

Wang, F., Qin, Z., Song, C., Tu, L., Karnieli, A., and Zhao, S. 2015. An improved mono-window algorithm for land surface temperature retrieval from Landsat-8 thermal infrared sensor data. Remote Sensing. 7: 4268-4289.

Wenbin, L., Yonghua, S., Dan, M., and Xiaojuan, L. 2013. Analysis of Beijing urban heat island under the influence of extreme heat based on HJ-1B data. Paper presented at the 2013 IEEE International Geoscience and Remote Sensing Symposium.

Weng, Q., and Fu, P. 2014. Modeling annual parameters of cleat-sky land surface temperature variations and evaluating the impact of cloud cover using time series of Landsat TIR Data. Remote Sensing of Environment. 140: 267-278.

Weng, Q., Fu, P., and Gao, F. 2014. Generating daily land surface temperature at Landsat resolution by fusing Landsat and Modis data. Remote Sensing of Environment. 145: 55-67.

Weng, Q., Lu, D., and Schubring, J. 2004. Estimation of land surface temperature-vegetation abundance relationship for urban heat island studies. Remote Sensing of Environment. 89: 467-483.

Wu, P., Shen, H., Ai, T., and Liu, Y. 2013. Land surface temperature retrieval at high spatial and temporal resolutions based on multi-sensor fusion. International Journal of Digital Earth. 6(1), 113-133.

Wu, P., Shen, H., Zhang, L., and Gottsche, F.M. 2015. Integrated fusion of multi-scale polar-orbiting and geostationary satellite observations for the mapping of high spatial and temporal resolution land surface temperature. Remote Sensing of Environment. 156, 169-181.

Zhou, J., Dai, F., Zhang, X., Zhao, S., and Li, M. 2015. Developing a temporally land cover-based look-up table (TL-LUT) method for estimating land surface temperature based on AMSE-E data over the Chinese landmss. International Journal of Applied Earth Observation and Geoinformation. 34: 35-50.